$A_y(\theta)$ for $\vec{p}$ + ^{208}Pb elastic scattering at 0.8 GeV and a test of multiple scattering theory

G. W. Hoffmann, L. Ray, M. Barlett, W. R. Coker, and J. McGill
University of Texas, Austin, Texas 78712

G. S. Adams,* G. J. Igo, F. Irom, A. T. M. Wang, and C. A. Whitten, Jr.
University of California, Los Angeles, California 90024

R. L. Boudrie and J. F. Amann
Los Alamos Scientific Laboratory, Los Alamos, New Mexico 87545

C. Glashausser
Rutgers University, New Brunswick, New Jersey 08903

N. M. Hintz and G. S. Kyle†
University of Minnesota, Minneapolis, Minnesota 55455

G. S. Blanpied
University of South Carolina, Columbia, South Carolina 29208
(Received 11 March 1981)

New, large-momentum-transfer 0.8 GeV $\vec{p}$ + ^{208}Pb elastic analyzing power data are presented and compared to optical model predictions using the Kerman-McManus-Thaler microscopic optical potential. This comparison provides an important test of multiple scattering theories since the predictions are quite sensitive to the assumed nucleon-nucleon scattering amplitudes and are not sensitive to the details of the nuclear densities. We show that improvement in the agreement between experiment and a parameter-free theoretical prediction is obtained when the calculation includes the electromagnetic spin-orbit potential which arises from the coupling of the projectile proton's magnetic moment and the Coulomb field of the target nucleus. The sensitivity of the predicted analyzing power to the various ingredients of the theory is also investigated, and the importance of the inclusion of target-nucleon correlations (in the second-order Kerman-McManus-Thaler potential) for proper explanation of the data is discussed.

[NUCLEAR REACTIONS ^{208}Pb($\vec{p}$,p), E = 0.8 GeV, measured $A_y(\theta)$; enriched target; resolution $\simeq$ 100 − 150 keV, $\theta_{c.m.}$ = 2° to 32°. Microscopic optical model analysis using second-order KMT potential; one-photon-exchange magnetic coupling included. Qualitative agreement between experiment and parameter-free calculation.]

I. INTRODUCTION

Common to many theories of proton-nucleus elastic scattering are microscopic descriptions of the scattering, in terms of nucleon-nucleon (N-N) amplitudes appropriate for the nuclear medium, and point-nucleon ground state matter densities. At medium energies ($E_{inc} \simeq 1$ GeV), because of the supposed validity of the impulse approximation, the effective nucleon-nucleon amplitudes should be those for free p-p and p-n scattering, so that realistic calculations can be made for comparison with experiment. For example, using the Kerman-McManus-Thaler (KMT) approach,[1,2] a microscopic optical potential can be generated for use in the

Schrödinger equation with relativistic kinematics.[3]

The availability of high quality 800 MeV $\vec{p}$ + nucleus elastic differential cross section and analyzing power data[3-7] has made possible a number of detailed, systematic studies of the adequacy of such microscopic descriptions of intermediate energy proton-nucleus scattering. Although the results obtained so far are encouraging,[7-9] calculations with *no* adjustable parameters have yet to be successful.[7,10]

One of the difficulties encountered in previous work[7-10] was the inability to compute, from first principles, analyzing powers which were in quantitative agreement with experiment, even at the very forward angles. Speculation on the reasons for this difficulty centered upon the possible lack of accurate knowledge of key amplitudes needed for the calculations; it was argued[8] that the needed amplitudes could not be determined from nucleon-nucleon data because a complete set of such data did not exist at relevant energies.

Thus, most of the reported analyses[4-9] of the 800 MeV $\vec{p}$ + nucleus elastic $A_y(\theta)$ data used an *empirical amplitude* for the isospin-averaged spin-dependent part of the nucleon-nucleon interaction. This Gaussian amplitude was adjusted from nucleus to nucleus[4-9] to obtain a best fit to the analyzing power data. Nonetheless, even with the additional degree of flexibility provided, the analyzing powers computed with the empirical Gaussian amplitudes were not in good quantitative agreement with experiment. An examination of the fits to data for target nuclei ranging from ^{12}C to ^{208}Pb reveals significant systematic differences between computed and experimental values.[4-9] These discrepancies, which exist at both small and large angles, are disturbing and are investigated in this work.

In order to provide more and better quality data for our investigation, the 800 MeV $\vec{p}$ + ^{208}Pb elastic analyzing power data[4] were remeasured with improved statistical accuracy and extended to center-of-mass scattering angles greater than 32°. Here, we present the new data and the results of additional theoretical work which explores the sensitivity of the predicted analyzing powers to the various ingredients of the theory. When the electromagnetic one-photon-exchange contribution to the proton-proton spin-orbit amplitude,[11] as well as the target nucleon correlation contributions to the second-order optical potential,[8] are properly taken into account, a better description of the data results from impulse approximation predictions which utilize nucleon-nucleon amplitudes obtained from phase-shift analysis of nucleon-nucleon data.

Section II gives a brief description of experimental details, while Sec. III presents the results of the theoretical investigation. Section IV contains a summary of our findings.

II. EXPERIMENTAL

The high resolution spectrometer (HRS) at the Los Alamos Clinton P. Anderson Meson Physics Facility (LAMPF) was used to obtain analyzing power data for 800 MeV $\vec{p}$ + ^{208}Pb elastic scattering over the laboratory angular range of 2° to 32°. The region 2° – 12° was covered during one running cycle (cycle 22) when the available beam intensity was $\lesssim$0.2 nA, while the 14° – 32° data were obtained during the subsequent cycles 23 and 24 when variable intensity to 4 nA was available.

A 19.7 mg/cm^2 enriched foil (99.9%) was used as the target for the cycle 22 measurements, while 50 and 150 mg/cm^2 enriched foils (99.9%) were used for the cycle 23 and 24 runs. For each running cycle the overall experimental energy resolution ranged typically from 100 to 150 keV full width at half maximum (FWHM); beam energy was 800$\pm$0.5 MeV; and the overall experimental angular resolution was $\simeq$2 mr FWHM.

The HRS was moved in 1.5° increments during cycle 22 and 2.0° increments during cycles 23 and 24. The elastic data were sorted into $\simeq$0.2° angular bins (except at the largest angles). Since the acceptance of the HRS in the plane of scattering is about 1.75°, a relatively continuous distribution was obtained for the analyzing power. For each cycle the absolute zero of scattering angle was determined to $\pm$0.03° by comparing the locations of the minima in the differential cross section with those reported in Ref. 6. Relative integrated beam currents were determined using an ion chamber located approximately 1 m downstream of the target.

Beam polarization was reversed at the source every three minutes. Logic levels generated at the source were read by the HRS on-line data acquisition system to tag each recorded event according to beam polarization. In effect, two experiments were done simultaneously: one with beam polarization "up" and the other with beam polarization "down." This technique eliminated most systematic sources of error from the calculated analyzing powers. Other systematic errors not eliminated are related to changes in beam phase space and to changes in the angle of incidence of the beam on target, with polar-

ization reversal. Such changes have been studied in detail during previous polarized beam experiments using the HRS and were found to be small.[4]

The beam polarization was determined on line for each run using a beam line polarimeter[12] located about 10 m upstream of the target. Beam polarization was typically 75% during the course of the experiment.

For each angular bin, the elastic analyzing power $A_y(\theta)$ was computed as

$$A_y(\theta) = \frac{1}{P_B} \frac{\sigma\uparrow - \sigma\downarrow}{\sigma\uparrow + \sigma\downarrow} , \quad (1)$$

where P_B is the beam polarization and $\sigma\uparrow$ and $\sigma\downarrow$ are the relative cross sections of elastic scattering at angle θ when the beam spin direction is up and down, respectively.

The experimental data, along with theoretical curves to be discussed, are shown in Fig. 1. With the exception that a 5% difference in the magnitude of the maximum at 8.5° is present, the new data are consistent with, but statistically more accurate than, the data reported earlier[4] over the region of overlap (2°—20°). It is interesting that beyond 20° the upper bound of the envelope of the analyzing power no longer continues to rise, but remains constant at about 0.65.

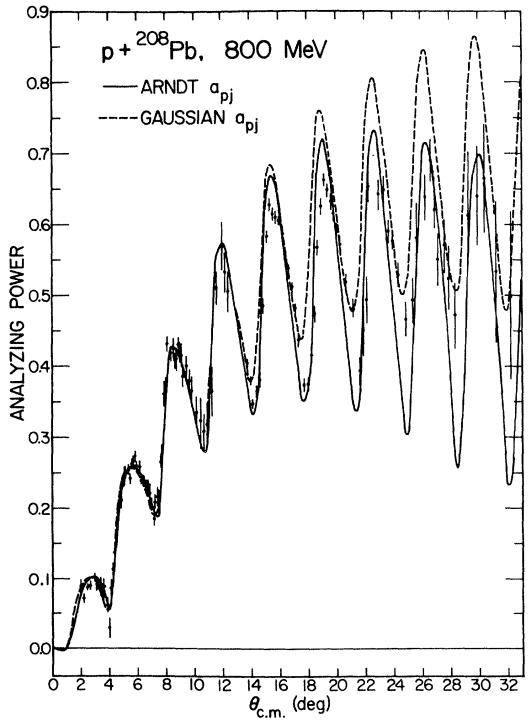

FIG. 1. Analyzing power data for 0.8 GeV $\vec{p}$ + ^{208}Pb elastic scattering. The curves are the results of phenomenological optical model calculations discussed in the text.

III. THEORETICAL

A. The model

The theoretical calculations employ the multiple scattering optical potential formalism of KMT.[1,2] The second-order, proton-nucleus KMT optical potential[2] is approximated by a local, spin-dependent form.[8] Solution of the Schrödinger equation with relativistic kinematics leads to the proton-nucleus observables.[8]

The input required to generate the second-order optical potential consists of: (1) proton and neutron one-body densities; (2) proton-nucleon spin-independent and spin-orbit scattering amplitudes[13]; and (3) the two-body target nucleon correlation function.[2,8]

The second-order contributions to the optical potential are approximated by local ρ^2 terms which account for Pauli, short-range dynamical, and center-of-mass correlations between the target nucleons.[8] The Pauli correlation contribution to the spin-orbit optical potential is also included.[8]

B. The densities

The proton density is obtained from the model-independent ^{208}Pb charge density[14] by unfolding the proton and neutron electric and magnetic form factors.[8,15] The neutron density is parametrized by the three-parameter Gaussian ($3pG$) form

$$\rho_n(r) = \rho_n{}^0(1 + w_n r^2/c_n{}^2)/\{1 + \exp[(r^2 - c_n{}^2)/z_n{}^2]\} \quad (2)$$

and, for a given set of proton-nucleon amplitudes, the parameters w_n, c_n, and z_n are adjusted to fit the 800 MeV $\vec{p}$ + ^{208}Pb differential cross section data.[6] Reasonable variations in the neutron density do not affect the shape or magnitude of the analyzing power predictions. *For this reason, a comparison of computed analyzing powers with data provides an important test of multiple scattering theories which rely on the impulse approximation.*

C. Nucleon-nucleon amplitudes

The general proton-nucleon scattering amplitude is written as[13]

$$f_{pj}(q) = a_{pj}(q) + b_{pj}(q)(\vec{\sigma}_j - \vec{\sigma}_p)\cdot\hat{n} + c_{pj}(q)(\vec{\sigma}_p + \vec{\sigma}_j)\cdot\hat{n} + \text{double spin-flip amplitudes} \ , \quad (3)$$

where q is the momentum transfer, $\hat{n}$ is the unit vector normal to the plane of scattering, and j refers to the target proton or neutron. The complex functions a_{pj}, b_{pj}, and c_{pj} contain contributions from both nuclear and electromagnetic interactions. For proton elastic scattering from a spin-zero nucleus, the double spin-flip terms do not contribute to the first order KMT potential, so that the amplitudes needed for input to the KMT calculations are

$$f_{pj}(q) = a_{pj}(q) + [c_{pj}(q) - b_{pj}(q)]\vec{\sigma}_p\cdot\hat{n} \ . \quad (4)$$

For p-p scattering, b_{pp} is identically zero because of particle exchange invariance. For p-n scattering, assuming charge independence, the nuclear part of b_{pn} is zero, but the electromagnetic part is not. The electromagnetic parts of c_{pp}, c_{pn}, and b_{pn}, whose physical origins trace to the coupling of the Coulomb field of the proton with the other nucleon's magnetic moment, have been calculated by Lechanoine *et al.*[11] using the one-photon-exchange approximation. In the limit $q^2 \to 0$ these amplitudes are proportional to $|q|^{-1}$. Furthermore, the c_{pn} and b_{pn} electromagnetic amplitudes are equal in sign and magnitude for $q^2 \to 0$. Thus, the most general amplitudes required for KMT calculations of proton-nucleus elastic scattering from a spin-zero nucleus can be written as

$$f_{pp}(q) = a_{pp}^{C}(q) + a_{pp}^{CN}(q) + [c_{pp}^{C}(q) + c_{pp}^{CN}(q)]\vec{\sigma}_p\cdot\hat{n} \ , \quad (5)$$

and

$$f_{pn}(q) = a_{pn}(q) + c_{pn}^{CN}(q)\vec{\sigma}_p\cdot\hat{n} \ , \quad (6)$$

where $a_{pn}(q) \simeq a_{pn}^{CN}(q)$. The a_{pp}^{C} and c_{pp}^{C} are purely electromagnetic amplitudes, while a_{pp}^{CN}, c_{pp}^{CN}, a_{pn}^{CN}, and c_{pn}^{CN} are Coulomb-distorted nuclear amplitudes. The first term on the right-hand side of Eq. (5) gives rise to the spin-independent Coulomb potential.[16] The Coulomb-distorted nuclear amplitudes give rise to the spin-independent and spin-orbit nuclear optical potentials.[8] The c_{pp}^{C} amplitude will generate an electromagnetic proton-nucleus spin-orbit potential through interaction of the incoming proton's magnetic moment with the Coulomb field of the nuclear charge distribution. This spin-orbit term was not included in previous KMT calculations[4–10] because phenomenological c_{pj}^{CN} amplitudes were invariably used to fit the proton-nucleus analyzing power data, and also because the effects of such a term were thought to be negligible. However, recent theoretical work[17] suggests that this term should be included in realistic calculations. As discussed later in this paper inclusion of this electromagnetic spin-orbit amplitude leads to a much improved microscopic description of the new 800 MeV $\vec{p}$ + ^{208}Pb analyzing power data, a result not found in Ref. 17.

All optical model calculations discussed have made use of the KMT No. 3 prescription which amounts to an approximate method of accounting for the Coulomb phase in $a_{pp}^{C}(q)$ [see Eq. (5)] in KMT calculations of the scattering amplitude.[16] According to this prescription, the spin-independent proton-nucleus amplitude is expressed as a sum of the Coulomb scattering amplitude for the full, distributed nuclear charge and a Coulomb-distorted nuclear amplitude.

D. Phenomenological and parameter-free results without electromagnetic spin-orbit amplitude

The previous KMT calculations[4–9] for $\vec{p}$ + nucleus analyzing powers at 800 MeV were done using N-N nuclear amplitudes parametrized according to

$$a_{pj}^{CN}(q) = (k_0\sigma_{pj}/4\pi)(i + \alpha_{pj})\exp(-B_{pj}q^2) \ ,$$
$$\mathrm{Re}[c_{pj}^{CN}(q)] = -(\hbar c k_0/8\pi Mc^2)\theta_{pj} q \exp(-B_{spj}^{\mathrm{Re}}q^2) \ , \quad (7)$$

and

$$\mathrm{Im}[c_{pj}^{CN}(q)] = (\hbar c k_0/8\pi Mc^2)\theta_{pj}\alpha_{spj} \times q \exp(-B_{spj}^{\mathrm{Im}}q^2) \ ,$$

where j = proton or neutron, k_0 is the N-N center-of-momentum system wave number, M is the nucleon mass, and q is the magnitude of the momentum transfer. The only electromagnetic potential considered was the usual static Coulomb potential generated by a_{pp}^{C}.[16] The parameters of Eq. (7) were obtained[8] by directly fitting the N-N cross section and polarization data under the assumption that the double spin-flip amplitudes were zero. However, use of these amplitudes in the KMT calculations resulted[4–9] in predicted proton-nucleus analyzing powers which were in poor agreement with data. The parameters of $\overline{c}_p$ (i.e.,

TABLE I. Effective spin-orbit amplitude parameters.[a]

Fit	$\bar{\theta}_p$ (fm^2)	$\bar{\alpha}_{sp}$	$\bar{B}_{sp}^{Re}$ (fm^2)	$\bar{B}_{sp}^{Im}$ (fm^2)
Using Arndt[b] a_{pj}^{CN}	4.25	1.90	0.33	0.48
Using Gaussian[c] a_{pj}^{CN}	6.46	1.19	0.30	0.30

[a]Where $c_{pp}^{CN} = c_{pn}^{CN}$ and $\bar{\theta}_p = \theta_{pp} = \theta_{pn}$, $\bar{\alpha}_{sp} = \alpha_{spp} = \alpha_{spn}$, $\bar{B}_{sp}^{Re} = B_{spp}^{Re} = B_{spn}^{Re}$, and $\bar{B}_{sp}^{Im} = B_{spp}^{Im} = B_{spn}^{Im}$.
[b]See solid curve of Fig. 1.
[c]See dashed curve of Fig. 1.

$\bar{c}_p = c_{pp}^{CN} = c_{pn}^{CN}$, and assuming $\bar{B}_{sp}^{Re} = \bar{B}_{sp}^{Im}$) were therefore varied for each nucleus in order to optimize the fits to the proton-nucleus analyzing power data.[4–10] Needless to say, the effective $\bar{c}_p$ amplitudes did not adequately describe the N-N data.[8]

The result of a similar calculation, using the empirical $a_{pj}^{CN}(q)$ amplitudes of Ref. 8, with $\bar{c}_p$ adjusted to optimize the fit to the new data in the angular range forward of 15°, is shown as the dashed curve in Fig. 1. As previously observed,[4–9] the second-order KMT prediction is consistently larger than the experimental $A_y(\theta)$ by an amount increasing with increasing angle past 20°. While the envelope of the experimental $\vec{p}$ + ^{208}Pb $A_y(\theta)$ has leveled off by 19°, the calculated $A_y(\theta)$ is still increasing at 30°. The condition $\bar{B}_{sp}^{Re} = \bar{B}_{sp}^{Im}$ was not imposed during the optimization, but was found to give the best fit (see Table I).

The a_{pj}^{CN} and c_{pj}^{CN} amplitudes of Arndt's phase shift solution[18] SM80 were then used for p-p and p-n to generate the local, second-order KMT optical potential. The prediction for the analyzing power is shown by the dashed curve in Fig. 2 and is quite different from the result (dashed curve of Fig. 1) obtained using the phenomenological amplitudes. The envelope of the calculated analyzing power follows that of the data fairly well, but fails to reproduce the *forward angle* diffractive structure.

Another calculation was then made using the a_{pp}^{CN} and a_{pn}^{CN} amplitudes of SM80 and empirically adjusted Gaussian amplitudes [as in Eq. (7)] for the isospin-averaged $\bar{c}_p$ (see Table I). The result, indicated by the solid curve of Fig. 1, reproduces most features of the data over the entire angular range.

The spin-independent $a_{pj}^{CN}(q)$ amplitudes used to generate the two curves shown in Fig. 1 and the dashed curve of Fig. 2 are shown in Fig. 3. The dominant imaginary parts of the phase shift amplitudes are similar to the corresponding parts of the Gaussian amplitudes, but the phase-shift-generated amplitudes have a slightly smaller range in momentum-transfer space. The *small,* real parts of the phase shift and Gaussian a_{pj}^{CN} are quite different,

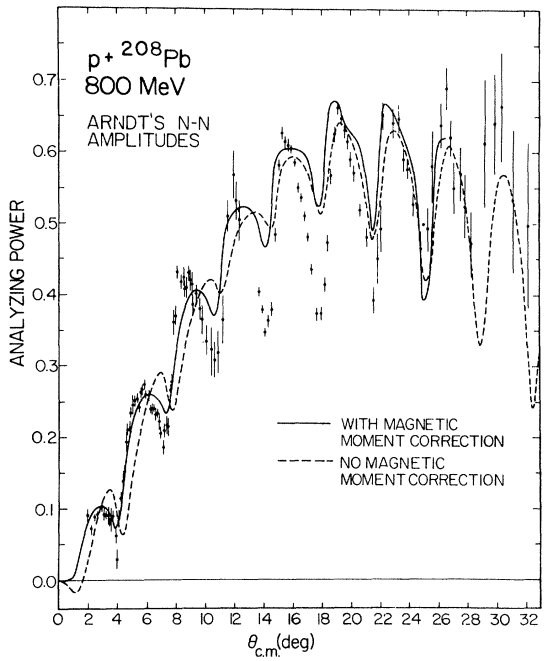

FIG. 2. The analyzing power data for 0.8 GeV $\vec{p}$ + ^{208}Pb elastic scattering are compared to KMT predictions obtained using nucleon-nucleon amplitudes obtained from phase shift analysis of nucleon-nucleon data. The effect of the one-photon-exchange contribution to $c_{pp}(q)$ is seen by comparing the solid and dashed curves (see text).

especially for $p + p$. Differences include shape, magnitude, and even algebraic sign.

In Fig. 4 we compare the spin-dependent $\bar{c}_p$ amplitudes used to generate the solid curve of Fig. 1 (see Table I) and the dashed curve of Fig. 2. Here the phase shift $\bar{c}_p$ amplitude is defined as $\bar{c}_p = [(Z/A)\, c_{pp}^{CN}(q) + (N/A)c_{pn}^{CN}(q)]$ in order to make the comparison. The gross discrepancies between effective and free, spin-dependent amplitudes seen in Fig. 4 suggest that an important aspect of physics is left out of the parameter-free calculation. We note, however, that *all* calculations discussed give essentially equivalent fits to the differential cross section data for 800 MeV $\vec{p}$ + ^{208}Pb elastic scattering. A typical fit (see also Ref. 16) is shown in Fig. 5. Below we show that a calculation that includes the electromagnetic spin-orbit potential arising from c_{pp}^{C} is able to remove much of the discrepancy between experiment and theory.

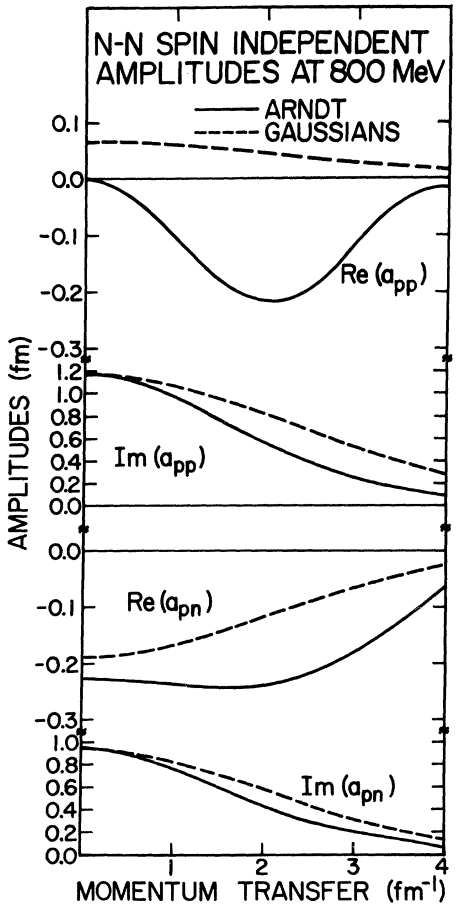

FIG. 3. A comparison of the spin-independent amplitudes (a_{pj}^{CN}) used for the calculations leading to the curves of Fig. 1.

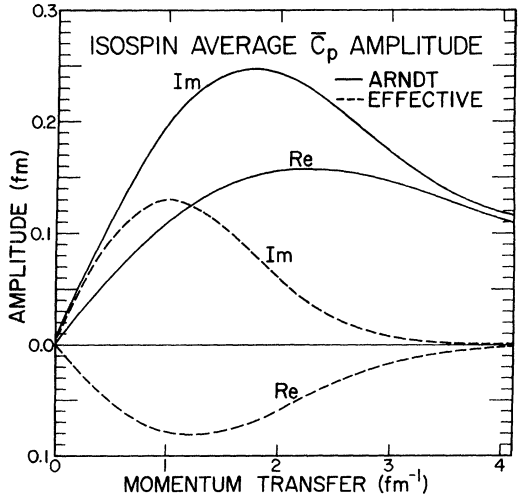

FIG. 4. The phenomenological isospin-averaged amplitude ($\bar{c}_p$) is compared to $[(Z/A)c_{pp}^{CN}(q) + (N/A)c_{pn}^{CN}(q)]$, where c_{pp}^{CN} and c_{pn}^{CN} are amplitudes predicted by phase shift analysis of nucleon-nucleon data.

E. Consideration of electromagnetic spin-orbit amplitude

An option of Arndt's phase shift code[18] allows nucleon-nucleon amplitudes to be generated using the electromagnetic amplitudes of Ref. 11. The 800 MeV c_{pp} amplitudes of solution SM80, generated with and without the electromagnetic contribution included, are shown in Fig. 6. The $|q|^{-1}$ behavior of $c_{pp}^{C}(q)$ at small q leads to a long-range proton-

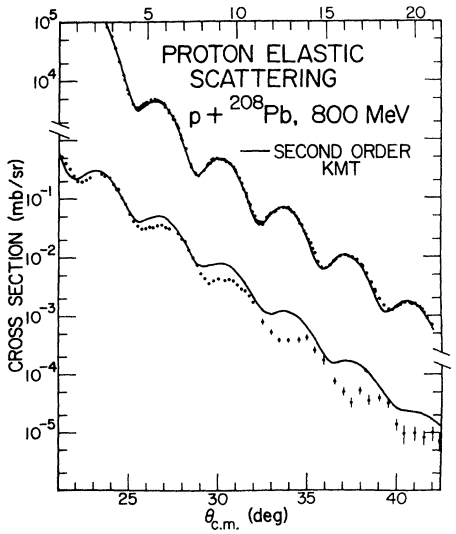

FIG. 5. Typical fit to the 800 MeV $\vec{p}$ + ^{208}Pb elastic angular distribution.

nucleus spin-orbit potential which is proportional to r^{-3} at large r ($r \gtrsim 2R_N$, where R_N is the nuclear radius). Since Coulomb wave functions corresponding to the spin-dependent Coulomb potential, $V_C(r) = Ze^2/r + (B_{so}/r^3)(\vec{\sigma}\cdot\vec{l}\,)$, are not known, the numerically generated wave functions corresponding to the full KMT optical potential must in principle be extended to a very large radius before they can be properly matched to the usual spin-independent Coulomb wave functions. Rather than carry out this very cumbersome calculation, we have made use of a convergence factor technique to obtain the theoretical analyzing power with the electromagnetic spin-orbit coupling included.

By multiplying the complex spin-orbit potential $V_S(r)$ by $\exp[-\alpha(r - r_{so})^2]$, we obtained the analyzing power as a function of convergence parameter α, or $A_y(\theta,\alpha)$, and extrapolation to $\alpha = 0$ gave the final analyzing power $A_y(\theta,\alpha = 0)$. To determine the general functional form of $A_y(\theta,\alpha)$ with respect to the convergence parameter α, several Glauber model[19] calculations were made to study the behavior of $A_y(\theta,\alpha)$ for small α. Writing the local optical potential in the form

$$V(r) = V_N(r) + V_S(r)\vec{\sigma}\cdot\vec{l} + V_{\text{Coul}}(r) \ , \qquad (8)$$

where $V_{\text{Coul}}(r)$ is the spin-independent proton-nucleus Coulomb potiental, the proton-nucleus scattering amplitude

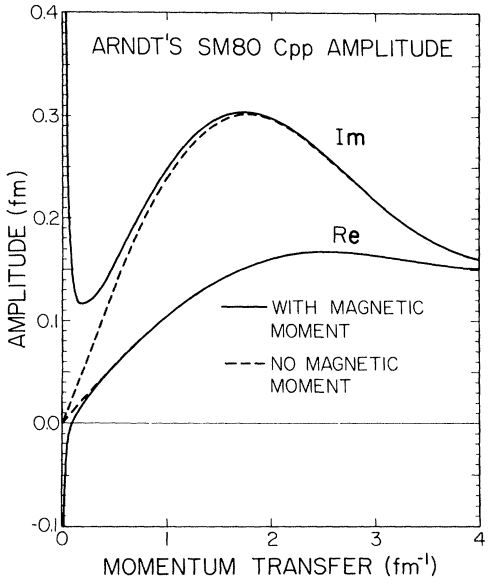

FIG. 6. The proton-proton spin-orbit amplitudes c_{pp} (solid curves) and c_{pp}^{CN} (dashed curves) of phase shift solution SM80. The differences between the two sets of curves are due to the pure electromagnetic one-photon-exchange contribution c_{pp}^{C}.

$$F(q) = f(q) + g(q)\vec{\sigma}\cdot\hat{n} \qquad (9)$$

is given in the Glauber model by[19,20]

$$f(q) = f_R(q) + ik\int_0^\infty db\, bJ_0(qb)e^{i\chi_{\text{pt}}(b)}\{1 - e^{i[\chi_C(b)+\chi_N(b)]}\cos[kb\chi_S(b)]\} \qquad (10)$$

and

$$g(q) = ik\int_0^\infty db\, bJ_1(qb)e^{i\chi_{\text{pt}}(b)}e^{i[\chi_C(b)+\chi_N(b)]}\sin[kb\chi_S(b)] \ . \qquad (11)$$

Here, k is the incident momentum, b is the impact parameter,[19] $f_R(q)$ is the Rutherford amplitude, $\chi_{\text{pt}}(b)$ and $\chi_C(b)$ are the point and distributed Coulomb phases defined in Ref. 20, and $\chi_N(b)$ and $\chi_S(b)$ are given by[19]

$$\chi_N(b) = -(\hbar v)^{-1}\int_{-\infty}^{\infty} dz' V_N(\vec{b} + \hat{k}z') \ , \qquad (12)$$

$$\chi_S(b) = -(\hbar v)^{-1}\int_{-\infty}^{\infty} dz' V_S(\vec{b} + \hat{k}z') \ , \qquad (13)$$

where v is the incident velocity. If the long range tail of $V_S(r)$ is expressed as

$$V_S(r) = B_{so}/r^3, \ \text{for } r > R_{\max} \ , \qquad (14)$$

where $R_{\max} \geq 2R_N$, then

$$\chi_S(b) = -2B_{so}/(\hbar v b^2), \ b > R_{\max}$$
$$= -(2/\hbar v)\int_0^{(R_{\max}^2 - b^2)^{1/2}} dz' V_S(\vec{b} + \hat{k}z')$$
$$- (2B_{so}/\hbar v)\,[b^{-2} - (R_{\max}^2 - b^2)^{1/2}(R_{\max}b^2)^{-1}], \ b \leq R_{\max} \ . \qquad (15)$$

For the case considered here, $kb\chi_S(b) << 1$ for $b > R_{max}$, so the scattering amplitudes in Eqs. (10) and (11) are readily evaluated. The contribution to the integral in Eq. (10) for $R_{max} \leq b \rightarrow \infty$ was shown to be negligible. The part of the integral in Eq. (11) for $R_{max} \leq b \rightarrow \infty$,

$$I(q) = -ik \int_{R_{max}}^{\infty} db\, bJ_1(qb) e^{i\chi_{pt}(b)} \times \sin[2B_{so}k/(\hbar v b)] \ , \quad (16)$$

was evaluated numerically. Thus, using the Glauber model and the KMT optical potential with the convergence factor, the $\vec{p} + {}^{208}$Pb analyzing powers $A_y(\theta,\alpha)$ were computed for $\alpha = 0$ and for various $\alpha > 0$. In this way, the convenience with which the Glauber formalism yields $A_y(\theta,\alpha = 0)$ was exploited to guide in the selection of convergence parameters for the full KMT calculations.

The variation of $A_y(\theta,\alpha)$ with α was found to be smooth, and values of $\alpha = 0.01$, 0.02, and 0.03 fm^{-2} (with $r_{so} = 6.6$ fm) were determined to be sufficiently small to permit an accurate parabolic extrapolation of the Schrödinger equation solutions for $A_y(\theta,\alpha)$ to $\alpha = 0$. A matching radius of 19.6 fm and 145 partial waves were required for these calculations.

The effect of the electromagnetic spin-orbit contribution to $c_{pp}(q)$ on the 800 MeV $\vec{p} + {}^{208}$Pb $A_y(\theta)$ can be seen by comparing the solid and dashed curves of Fig. 2. The differences between the two curves are surprising. Including the electromagnetic contribution to $c_{pp}(q)$ shifts the angular positions of the maxima and minima in the predicted analyzing power into alignment with the data at all forward angles where previous calculations (e.g., dashed curve of Fig. 2) have failed. The data forward of 8° are now qualitatively reproduced by the parameter-free prediction. There is still not enough structure predicted between 8° and 20°, but at least the diffractive pattern is now in alignment with the data.

The importance of the electromagnetic spin-orbit potential indicates that phenomenological c_{pp} amplitudes should include this $|q|^{-1}$ dependence in addition to the $q \exp(-Bq^2)$ form of Eq. (7). We anticipate that the c_{pp}^{CN} part of an empirical c_{pp} amplitude which includes the $|q|^{-1}$ dependence at $q^2 \rightarrow 0$ will be similar to the phase shift results displayed in Fig. 4.

To close the discussion of this topic, we note that a previously reported eikonal calculation by Osland and Glauber[17] first suggested the importance of the electromagnetic spin-orbit potential for proton elastic scattering at medium energies. However, their results are quantitatively different from those reported here. In particular, including the electromagnetic spin-orbit term led to a shift to *larger* angle of the position of the first maximum in the analyzing power with no change in position for the first minimum.[17] We also comment that a previously reported preliminary KMT calculation[21] of proton-nucleus analyzing powers at 800 MeV, using phase shift amplitudes with the electromagnetic spin-orbit term included, is incorrect due to an insufficiently large matching radius used in joining the numerical solutions to the Coulomb wave functions.

F. Sensitivity to uncertainty in nucleon-nucleon amplitudes

The remaining discrepancy between experiment and theory (solid curve in Fig. 2) occurs near the third and fourth maxima in $A_y(\theta)$, or at about 1.5 fm^{-1}. The part of $c_{pj}^{CN}(q)$ which dominates the proton-nucleus analyzing powers at 1.5 fm^{-1} lies between $q = 0$ and $q \simeq 1.5$ fm^{-1}. Since forward-angle ($0 \leq q \lesssim 1.5$ fm^{-1}) N-N data at or near 800 MeV are scarce,[18,22] especially for p-n, the discrepancy may very well reflect inaccurately determined N-N amplitudes at small momentum transfers. Forward angle (6° – 30° in c.m.) 800 MeV p-p and p-n triple scattering measurements will be made in the near future at LAMPF to provide the required data to check the adequacy of the phase shift predictions at small q.

To investigate whether small variations in one or more of the needed amplitudes could significantly improve the prediction shown in Fig. 2, three different sets of amplitudes were generated for sensitivity calculations. The first set consisted of a_{pp}^{CN} and c_{pp}^{CN} from phase shift solution SM80 and a_{pn}^{CN} and $\mathrm{Im}(c_{pn}^{CN})$ from solution CK80, but with a Gaussian $\mathrm{Re}(c_{pn}^{CN})$ obtained as in Ref. 8 by searching to minimize the total chi squared for the available $p + n$ cross section and polarization data.[12] In this search, a_{pn}^{CN}, $\mathrm{Im}(c_{pn}^{CN})$, and the other Wolfenstein amplitudes,[13] m_{pn}, g_{pn}, and h_{pn}, were taken from CK80 and held fixed. The second set of amplitudes consisted of a_{pp}^{CN} and c_{pp}^{CN} from SM80, and a_{pn}^{CN}, $\mathrm{Re}(c_{pn}^{CN})$, m_{pn}, g_{pn}, and h_{pn} of CK80, with $\mathrm{Im}(c_{pn}^{CN})$ varied to fit the $p + n$ data. The third set of amplitudes consisted of a_{pp}^{CN} and c_{pp}^{CN} from SM80 and Gaussian a_{pn}^{CN} and c_{pn}^{CN}, with m_{pn}, g_{pn}, and h_{pn} from CK80. The Gaussian amplitudes were searched to fit the $p + n$ data, using the form of Eq. (7).

In this way, by constraining some of the amplitudes to be those predicted by phase shift solutions,

and independently adjusting others to refit the N-N data, we were able to generate a variety of "new" solutions which fit the $p + n$ angular distribution and polarization data with chi-squared values equal to or superior to those of the phase shift solutions. The resulting Gaussian amplitudes generally tend to agree well with Arndt's phase shift generated amplitudes, but give slightly different predictions for the 800 MeV $\vec{p}$ + ^{208}Pb analyzing power. The primary differences lie in the overall magnitude predicted, and in the depths predicted for the minima. Typical changes in $A_y(\theta)$ are 0.02 at forward angles and 0.05 at larger angles. Noting that the new amplitudes were generated using the *same* m_{pn}, g_{pn}, and h_{pn} double spin-flip amplitudes (which may themselves be poorly determined), it is possible that the remaining differences between theory and data (Fig. 2) are due to slightly inaccurate N-N amplitudes at low q.

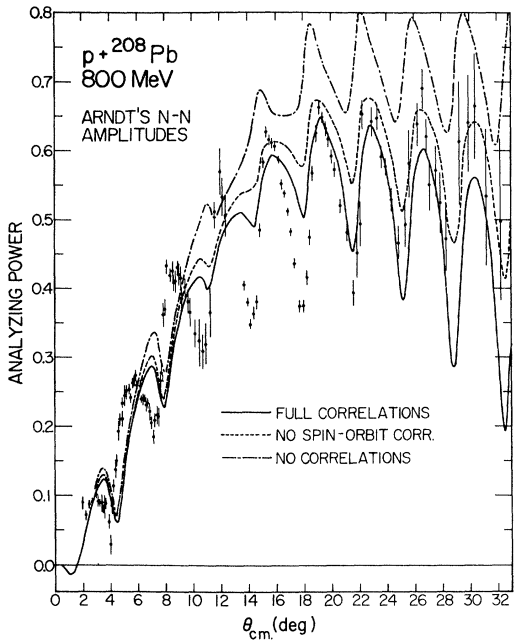

FIG. 7. The 0.8 GeV $\vec{p}$ + ^{208}Pb elastic analyzing power data are compared to results of calculations done using amplitudes resulting from phase shift analysis of nucleon-nucleon data. The three curves shown illustrate the importance of two-nucleon correlations (see text). The electromagnetic spin-orbit potential was omitted in these calculations.

G. Sensitivity to nucleon-nucleon correlations

The calculations reported here also include local ρ^2 approximations for the generally nonlocal, second-order KMT optical potential.[8] In Fig. 7 the effects of these correlation contributions on the predicted analyzing power are shown. In each calculation, the electromagnetic spin-orbit potential was omitted and the fit to the differential cross section data was recovered by slightly varying the neutron density parameters. The dashed-dotted curve resulted when no correlations were included. The dashed curve was obtained by including Pauli, short-range dynamical, and center-of-mass correlation contributions to the spin-independent part of the optical potential. The solid curve was obtained by additionally including the Pauli correction to the spin-orbit potential.[8] However, the derivation of the simple ρ^2 form of the second-order optical potential term uses the eikonal and local density approximations and assumes that the correlation and N-N interaction ranges (typically 0.5 and 1 fm, respectively) are small compared to the nuclear size; thus, the good fit at back angles (solid curve in Fig. 2) *may* be fortuitous. The differences between the three curves in Fig. 7 provide an estimate of the second-order correlation effects.

An additional calculation was made using the empirical $\bar{c}_p$ amplitude of Table I to generate the spin-orbit correlation potential. The differences between the resulting $A_y(\theta)$ of the KMT calculation and the analogous calculation using the phase shift c_{pj}^{CN} are somewhat significant in that the depths of the minima vary by as much as 0.03. Thus, we cannot discount the possibility that part of the remaining discrepancy between theory and experiment may be due to the inexact treatment of correlations.[8]

H. Other considerations

Calculations were also made in which the Coulomb distorted nuclear parts of the N-N amplitudes were more carefully transformed from the N-N c.m. system to the proton-nucleus Breit system.[23] The differences between such amplitudes and those obtained by transforming each part of the amplitudes of Eq. (3) as if they were simply scalars (as done for the standard calculations reported in this paper and others[3-9]) are that the range of $\mathrm{Im}[a_{pj}^{CN}(q)]$ in momentum-transfer space is increased, and the nucleon c.m. system amplitude $c_{pj}^{CN}(\vec{\sigma}_p + \vec{\sigma}_j)\cdot\hat{n}$ becomes $(c_p^{CN'}\vec{\sigma}_p + c_j^{CN'}\vec{\sigma}_j)\cdot\hat{n}$ in the Breit frame. Wallace obtained[23] a Gaussian parametrization of the properly transformed nuclear amplitudes of Arndt's phase shift solution CD79, as

well as a Gaussian parametrization of the CD79 center-of-mass amplitudes. Using these two amplitude sets, we then obtained new predictions for the 800 MeV $\vec{p}$ + ^{208}Pb analyzing power. The main effect observed was a slight deepening of the minima of $A_y(\theta)$ by amounts varying from 0.01 (at 10°) to 0.05 (at larger angles).

Additional corrections to the impulse approximation remain to be evaluated. Although the spin-independent effects of Pauli blocking,[24] Fermi motion averaging,[25] and nonlocality[26] have been estimated to be small,[27] the spin-dependence of these corrections to the impulse approximation has not been considered. Other possibly important corrections include off-shell effects[8] and additional Coulomb effects,[16] as well as the proper relativistic transformation of the full Coulomb plus nuclear N-N amplitudes from the c.m. to the Breit frame. Such a transformation *would mix* Coulomb and nuclear terms and could have nonnegligible consequences for nuclear size determination and analyzing power predictions. The latter question is presently under investigation.

I. Spin-rotation predictions

Finally, KMT predictions for the spin-rotation quantity[28] $Q(\theta)$, corresponding to the various calculations discussed in this work, are shown in Fig. 8. The solid curve corresponds to the calculation which generated the dashed curve of Fig. 2 (p-p and p-n nuclear amplitudes from phase shift solution SM80, no electromagnetic spin-orbit term), while the dashed-dotted curve corresponds to the solid curve of Fig. 2 [p-p and p-n nuclear amplitudes from phase shift solution SM80, with $c_{pp}^{C}(q)$ included]. The dashed curve is the prediction using a_{pp}^{CN} and a_{pn}^{CN} from SM80 and the empirical $\bar{c}_p$ of Table I (corresponding to the solid curve of Fig. 1). The large differences between the solid or dashed-dotted curves and the dashed curve are due to the large differences in the Re[$\bar{c}_p(q)$] used for each calculation (see Figs. 4 and 6). The significant differences between the solid and dashed-dotted curves are due to the electromagnetic spin-orbit potential. Since the predicted spin-rotation parameter is affected by both Re[$c_{pj}^{CN}(q)$] and $c_{pp}^{C}(q)$, measurement of $Q(\theta)$ will provide an additional constraint for evaluating the success of microscopic calculations at 800 MeV. In addition, measurement of the three observables, $d\sigma/d\Omega$, $A_y(\theta)$, and $Q(\theta)$, provides all the information required to obtain the proton-nucleus amplitudes at each q (except for an overall phase).

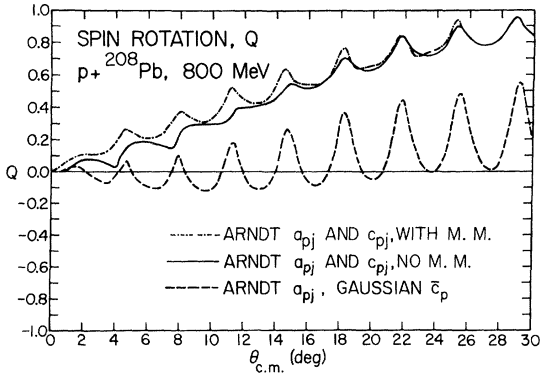

FIG. 8. Second-order KMT predictions of the spin-rotation quantity $Q(\theta)$. The three curves resulted using the same phase shift generated a_{pj}^{CN} amplitudes, but different spin-dependent c_{pj} amplitudes (see text).

IV. SUMMARY AND CONCLUSION

New 800 MeV $\vec{p}$ + ^{208}Pb elastic analyzing power data have been presented and analyzed. It was shown that a second-order, parameter-free KMT prediction obtained using currently available N-N amplitudes, the impulse approximation, and the electromagnetic spin-orbit potential (arising from the coupling of the incident proton's magnetic moment with the Coulomb field of the target nucleus) provides a qualitative description of the data. The leveling off of the analyzing power envelope at a value of 0.65 for angles greater than 20° is correctly predicted by the best microscopic calculation, and the locations of the predicted maxima and minima agree with the data. The sensitivity of the predicted $A_y(\theta)$ to N-N amplitude uncertainties and to second-order correlation contributions was found to be significant. These uncertainties could possibly account for the remaining discrepancy between the best microscopic prediction and the data.

Estimates of the effect on $A_y(\theta)$ of the proper relativistic transformation of the nuclear N-N amplitudes from the N-N center-of-mass to the Breit frame were made, and the effect was found to be small. Finally, predictions for the spin-rotation quantity, $Q(\theta)$ were obtained using both phase shift and phenomenological amplitudes.

Very recently, we have also conducted a preliminary investigation of electromagnetic spin-orbit effects in 800 MeV $\vec{p}$ + ^{40}Ca elastic scattering. A

substantially improved fit to the forward-angle $A_y(\theta)$ data was obtained when the electromagnetic spin-orbit potential was included.

This work was supported in part by the U. S. Department of Energy and The Robert A. Welch Foundation.

---

*Present address: Bates Laboratory, Massachusetts Institute of Technology, Cambridge, Massachusetts 02139.
†Present address: SIN, 5234 Villigen, Switzerland.

[1]A. K. Kerman, H. McManus, and R. M. Thaler, Ann. Phys. (N.Y.) 8, 551 (1959).
[2]H. Feshbach, A. Gal, and J. Hüfner, Ann. Phys. (N.Y.) 66, 20 (1971).
[3]G. S. Blanpied *et al.*, Phys. Rev. Lett. 39, 1447 (1977).
[4]G. W. Hoffmann *et al.*, Phys. Rev. Lett. 40, 1256 (1978).
[5]G. W. Hoffmann *et al.*, Phys. Lett. 76B, 383 (1978).
[6]G. W. Hoffmann *et al.*, Phys. Rev. C 21, 1488 (1980).
[7]L. Ray *et al.*, Phys. Rev. C 23, 828 (1981).
[8]L. Ray, Phys. Rev. C 19, 1855 (1979).
[9]L. Ray, W. R. Coker, and G. W. Hoffmann, Phys. Rev. C 18, 2641 (1978).
[10]D. Hutcheon *et al.* (unpublished).
[11]C. Lechanoine, F. Lehar, F. Perrot, and P. Winternitz, Nuovo Cimento 56, 201 (1980).
[12]M. L. Barlett, Ph.D. thesis, The University of Texas at Austin, 1980 (unpublished).
[13]M. J. Moravcsik, *The Two-Nucleon Interaction* (Clarendon, Oxford, 1963), pp. 11–18.
[14]B. Frois *et al.*, Phys. Rev. Lett. 38, 152 (1977).
[15]W. Bertozzi, J. Friar, J. Heisenberg, and J. W. Negele, Phys. Lett. 41B, 408 (1972).
[16]L. Ray, G. W. Hoffmann, and R. M. Thaler, Phys. Rev. C 22, 1454 (1980).
[17]P. Osland and R. J. Glauber, Nucl. Phys. A326, 255 (1979).
[18]R. A. Arndt (private communication).
[19]R. J. Glauber, in *Lectures in Theoretical Physics,* edited by W. E. Brittin and L. G. Dunham (Interscience, New York, 1959), p. 315.
[20]I. Ahmad, Nucl. Phys. A247, 418 (1975).
[21]L. Ray, in *Polarization Phenomena in Nuclear Physics–1980 (Santa Fe),* Proceedings of the Fifth International Symposium on Polarization Phenomena in Nuclear Physics edited by G. G. Ohlsen, R. E. Brown, Nelson Jarmie, W. W. McNaughton, and G. M. Hale (American Institute of Physics, New York, 1980), p. 295.
[22]J. Bystricky, F. Lehar, and Z. Janout, Saclay Report No. CEA-N-1547(E), 1972 (unpublished).
[23]S. J. Wallace, Annu. Rev. Nucl. Sci. (to be published).
[24]E. Clementel and C. Villi, Nuovo Cimento 2, 176 (1955).
[25]J. W. Negele and D. Vautherin, Phys. Rev. C 5, 1472 (1972).
[26]B. Mulligan, Ann. Phys. (N.Y.) 26, 159 (1964).
[27]L. Ray (unpublished).
[28]R. J. Glauber and P. Osland, Phys. Lett. 80B, 401 (1979).